

Thermal analysis of synthetic reevesite and cobalt substituted reevesite $(\text{Ni,Co})_6\text{Fe}_2(\text{OH})_{16}(\text{CO}_3) \cdot 4\text{H}_2\text{O}$

Kathleen H. Bakon · Sara J. Palmer ·
Ray L. Frost

Received: 3 February 2009 / Accepted: 3 April 2009 / Published online: 19 June 2009
© Akadémiai Kiadó, Budapest, Hungary 2009

Abstract The mineral reevesite and the cobalt substituted reevesite have been synthesised and studied by thermal analysis and X-ray diffraction. The $d(003)$ spacings of the minerals ranged from 7.54 to 7.95 Å. The maximum $d(003)$ value occurred at around Ni:Co 0.4:0.6. This maximum in interlayer distance is proposed to be due to a greater number of carbonate anions and water molecules intercalated into the structure. This increase in carbonate anion content is attributed to an increase in surface charge on the brucite like layers. The maximum temperature of the reevesite decomposition occurs for the unsubstituted reevesite at around 220 °C. The effect of cobalt substitution results in a decrease in thermal stability of the reevesites. Four thermal decomposition steps are observed and are attributed to dehydration, dehydroxylation and decarbonation, decomposition of the formed carbonate and oxygen loss at ~807 °C. A mechanism for the thermal decomposition of the reevesite and the cobalt substituted reevesite is proposed.

Keywords Hydrotalcite · Brucite · Raman microscopy · Carrboydite · Hydrohonessite · Takovite · Mountkeithite

Introduction

Hydrotalcites have been known for an extended period of time [1–3]. Hydrotalcites, or layered double hydroxides (LDH) are fundamentally known as anionic clays [4]. The structure of hydrotalcite can be derived from a brucite

structure $(\text{Mg}(\text{OH})_2)$ in which e.g. Al^{3+} or Fe^{3+} (pyroaurite-sjögrenite) substitutes a part of the Mg^{2+} [2, 5–7]. This substitution creates a positive layer charge on the hydroxide layers, which is compensated by interlayer anions or anionic complexes. This surface charge is dependent upon the degree of substitution. In hydrotalcites a broad range of compositions are possible of the type $[\text{M}_{1-x}^{2+}\text{M}_x^{3+}(\text{OH})_2]_{x/n} \cdot y\text{H}_2\text{O}$, where M^{2+} and M^{3+} are the di- and trivalent cations in the octahedral positions within the hydroxide layers with x normally between 0.17 and 0.33. A^{n-} is an exchangeable interlayer anion [8]. There exists in nature a significant number of hydrotalcites which are formed as deposits from ground water containing Ni^{2+} and Fe^{3+} [9]. These are based upon the dissolution of Ni-Fe sulphides during weathering. Normally the hydrotalcite structure based upon takovite (Ni,Al) and hydrotalcite (Mg,Al) has basal spacings of ~8.0 Å where the interlayer anion is carbonate. If the carbonate is replaced by sulphate then the mineral carrboydite is obtained. Similarly reevesite is the (Ni,Fe) hydrotalcite with carbonate as the interlayer anion, which when replaced by sulphate the minerals honessite and hydrohonessite are obtained. Among the naturally occurring hydrotalcites are carrboydite and hydrohonessite [10, 11]. These two hydrotalcites are based upon the incorporation of sulphate into the interlayer with expansions of 10.34–10.8 Å.

Our interest in reevesite originates from the fact that reevesite and related minerals have been found in a wide range of deposits in Western Australia and also have been found in Shale balls resulting from the impact of a meteor with earth at Wolfe Creek (W.A.). When a meteorite crashed into earth, the impact can have devastating changes to the environment. Such a meteor of some estimated 50,000 tonnes crashed into a remote area of Western Australia some 300,000 years ago. The crater is some 875 m across and approximately 65 m deep. The impact of the meteor

K. H. Bakon · S. J. Palmer · R. L. Frost (✉)
Inorganic Materials Research Program, School of Physical
and Chemical Sciences, Queensland University of Technology,
GPO Box 2434, Brisbane, QLD 4001, Australia
e-mail: r.frost@qut.edu.au

can cause changes to the mineralogy of the district and surrounds [12–15]. In the case of the Wolfe creek meteorite fragments were scattered for over 4 km from the impact site. The impact can cause the formation of new minerals as a result of the high pressure and temperatures [16–18]. The meteor was originally an iron meteor containing both phosphorus and nickel [19]. Weathering of the meteor fragments has resulted in the formation of a range of new minerals due to oxidation and corrosion [19]. The meteor before impact in all probability contained the mineral schreibersite which with oxidation and hydration has completely changed to several phosphate minerals including lipscombite, cassidyite and collinsite [19]. Much of the original meteorite has weathered to goethite. The presence of Fe and Ni in the iron meteorite has resulted in the formation of a hydrotalcite reevesite. In the interior of some of the shale balls mineral formation of some of these above minerals has occurred. Faust et al. [20] published information on the formation of the mineral pecoraite [21, 22] in the crevices of the Wolfe creek shale balls. Faust et al. claimed the pecoraite was formed during mechanochemical weathering. This however seems unlikely and the question arises as to whether the mineral was formed during some form of extraterrestrial weathering. The question arises as to whether the weathering has occurred from the inside of the shale ball or if the weathering occurred through cracks and crevices from the outside.

Thermal analysis has been applied to the study of hydrotalcites [23–31]. An important study of these hydrotalcites is the thermal decomposition as this information provides concepts on the thermal stability of reevesite. This thermal stability is important in the assessment of whether the reevesite was formed in the shale balls before impact or whether the minerals are formed post-impact.

Experimental

Preparation of reevesite and Co doped reevesite

Reevesite and several Co doped reevesites were synthesised by the co-precipitation method. Two solutions were

made: solution 1 contained 2 M NaOH and 0.2 M Na₂CO₃, whilst solution 2 contained FeCl₃ · 6H₂O, NiCl₂ · 6H₂O and CoCl₂ · 6H₂O in ratios shown in Table 1. Solution 1 was added to solution 2 drop wise using a burette under vigorous stirring. The mixed solutions were left to stir for 24 h, and then vacuum filtered and washed with deionised water to remove any residual salts. The resulting paste was dried in an oven at 80 °C overnight.

X-ray diffraction

X-Ray diffraction patterns were collected using a Philips X'pert wide angle X-Ray diffractometer, operating in step scan mode, with Cu K_α radiation (1.54052 Å). Patterns were collected in the range 3–90° 2θ with a step size of 0.02° and a rate of 30 s per step. Samples were prepared as a finely pressed powder into aluminium sample holders. The Profile Fitting option of the software uses a model that employs twelve intrinsic parameters to describe the profile, the instrumental aberration and wavelength dependent contributions to the profile.

Thermal analysis

Thermal decomposition of the reevesite was carried out in a TA® Instruments incorporated high-resolution thermogravimetric analyzer (series Q500) in a flowing nitrogen atmosphere (80 cm³/min). Approximately 50 mg of sample was heated in an open platinum crucible at a rate of 2.0 °C/min up to 500 °C. The TGA instrument was coupled to a Balzers (Pfeiffer) mass spectrometer for gas analysis. Only selected gases such as water and carbon dioxide were analyzed.

Results and discussion

X-ray diffraction

The X-ray diffraction patterns of the synthesised reevesites and their d(003) spacings together with standard reference patterns are shown in Fig. 1. As the cobalt component of

Table 1 Table of the ratios of Ni and Co compounds for the synthesis of reevesite and cobalt doped reevesite

Ratio Ni:Co	Mole of NiCl ₂ · 6H ₂ O	Moles of CoCl ₂ · 6H ₂ O	Moles of FeCl ₃ · 6H ₂ O
1:0	0.075	0.000	0.025
0.8:0.2	0.060	0.015	0.025
0.6:0.4	0.045	0.030	0.025
0.4:0.6	0.030	0.045	0.025
0.2:0.8	0.015	0.060	0.025
0:1	0.000	0.075	0.025

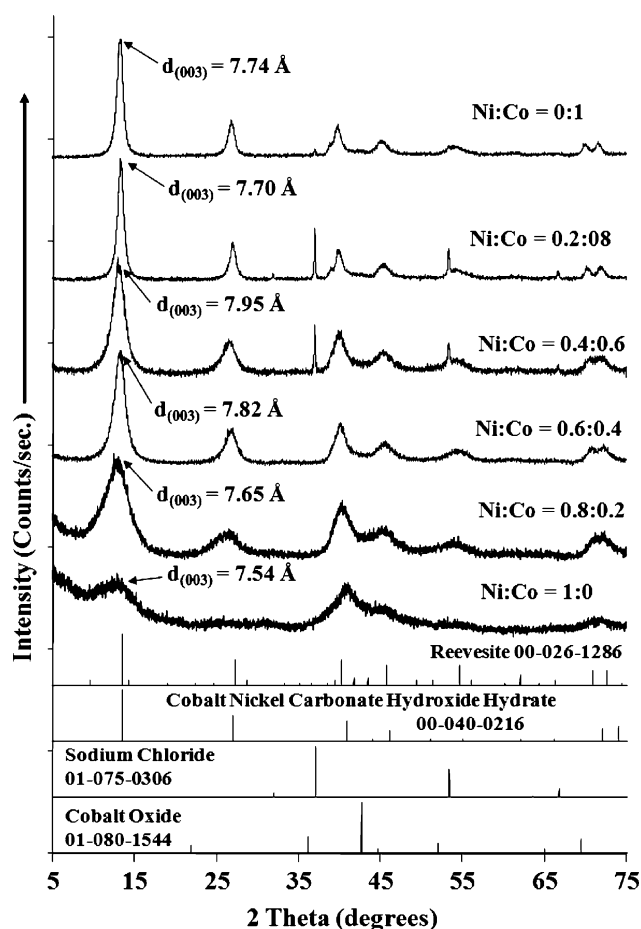


Fig. 1 X-ray diffraction of reevesite and cobalt doped reevesite and standards

the synthesised reevesites increased, X-ray diffraction peaks became sharper, indicating that the level of crystallinity of the mineral had also increased. The $d_{(003)}$ values also varied with composition, finding a maximum for Ni:Co = 0.4:0.6 reevesite, indicating that at this ratio the greatest interlayer distance is obtained. This increase in interlayer distance is proposed to be due to a greater number of carbonate anions and water molecules are intercalated into the structure. This increase can only be brought about through an increase in positive surface charge on the brucite-like surfaces. If some oxidation of Co(II) to Co(III) occurred then this would provide a mechanism for the increased positive surface charge. The Ni:Co = 0.6:0.4 also had a relatively high interlayer distance. It is proposed that at the 0.4:0.6 ratio, the nickel and cobalt interfere with each other's packing patterns, increasing the interlayer distance. The minimum $d_{(003)}$ value occurred for Ni:Co = 1:0, where the disappearance of cobalt caused the mineral layers to pack more closely together. However the interlayer distance also decreased from the 0.4:0.6 ratio with the reduction of nickel. With an increasing cobalt concentration, the $d_{(003)}$ peak appears to

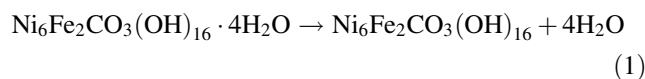
move to higher 2 theta positions. The width of the $d_{(003)}$ peak increases with cobalt substitution. This is indicative of a decrease in crystallinity.

Thermal analysis

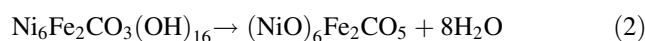
The thermogravimetric analysis of the synthesised reevesite without any substitution is shown in Fig. 2. A summary of the thermoanalytical results is provided in Table 2. Four thermal decomposition steps are observed at 52, 216, 515 and 807 °C. These mass loss steps are attributed to dehydration, dehydroxylation and decarbonation, decomposition of the formed carbonate and oxygen loss at 807 °C. The mass loss at these steps is 10.13%, 15.2%, 3.54% and 3.12%. Figure 3 displays the TG and DTG curves for reevesite with 20% Co substitution. Four mass loss steps are again observed at 45, 219, 550 and 791 °C with mass losses of 12.06%, 15.55%, 1.23% and 1.89%. Figure 4 shows the TG and DTG curves for reevesite with 40% Co substitution. The formula is $(\text{Ni}_{0.8}\text{Co}_{0.2})_6\text{Fe}_2(\text{OH})_{16}(\text{CO}_3) \cdot 4\text{H}_2\text{O}$. Four mass loss steps are observed at 65, 123, 226, 540 and 770 °C with mass losses of 10.69%, 16.89%, 1.23% and 3.32%. An additional mass loss step is observed at 123 °C. This step was not observed in Figs. 2 and 3. This decomposition is assigned to interlayer water held in the cobalt substituted reevesite. Figure 5 reports the TG and DTG curves for reevesite with 60% Co substitution. The formula is given by $(\text{Ni}_{0.4}\text{Co}_{0.6})_6\text{Fe}_2(\text{OH})_{16}(\text{CO}_3) \cdot 4\text{H}_2\text{O}$. Four mass loss steps are observed at ~72, 203, 500 and 812 °C with mass losses of 9.16%, 14.22%, 1.80% and 8.86%. Figure 6 records the TG and DTG curves for reevesite with 80% Co substitution $(\text{Ni}_{0.2}\text{Co}_{0.8})_6\text{Fe}_2(\text{OH})_{16}(\text{CO}_3) \cdot 4\text{H}_2\text{O}$. Four mass loss steps are observed at 63, 123, 193 and 872 °C with mass losses of 8.56%, 12.19% and 14.28%. Figure 7 displays the thermal analysis of cobalt reevesite $(\text{Co})_6\text{Fe}_2(\text{OH})_{16}(\text{CO}_3) \cdot 4\text{H}_2\text{O}$. Four mass loss steps are observed at 65, 116, 183 °C and two overlapping steps at 796 and 821 °C. This thermal analysis pattern resembles the TG-DTG patterns given in Figs. 4 and 6.

Mechanism of thermal decomposition

The following steps show the possible mechanism for the decomposition of reevesite mass loss step 1 at 52 °C:



Mass loss step 2 at 216 °C:



Mass loss step 3 at 515 °C:

Fig. 2 Thermogravimetric analysis of reevesite (100% Ni)

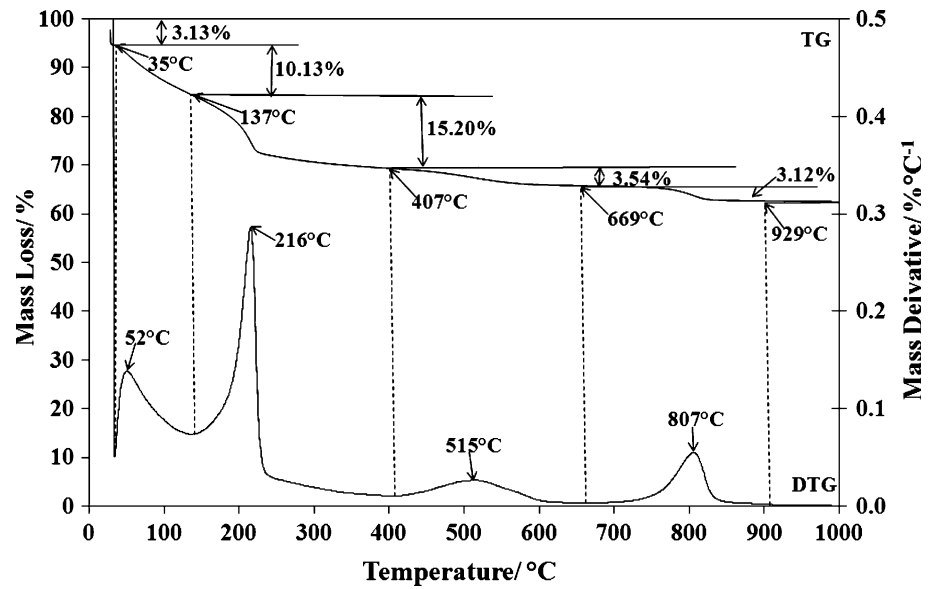


Table 2 Summary of the results of the Thermal analysis of reevesite and cobalt doped reevesite

Ni:Co 1:0		Ni:Co 0.8:0.2		Ni:Co 0.6:0.4		Ni:Co 0.4:0.6		Ni:Co 0.2:0.8		Ni:Co 0:1	
Temperature range (°C)	Mass loss %										
29–35	3.13	30–36	6.58	31–37	2.72	31–37	5.80	31–38	2.75	32–38	2.71
35–137	10.13	36–145	12.06	37–85	3.68	37–134	9.16	38–82	2.13	38–73	1.74
137–407	15.20	145–426	15.55	85–150	7.01	134–380	14.22	82–140	8.56	73–133	9.80
407–669	3.54	426–646	1.23	150–447	16.89	380–626	1.80	140–367	12.19	133–348	13.11
669–929	3.12	646–889	1.89	447–873	3.32	626–885	8.86	367–859	14.28	348–666	1.14
										666–892	5.67

Fig. 3 Thermogravimetric analysis of 20% cobalt doped reevesite (80% Ni)

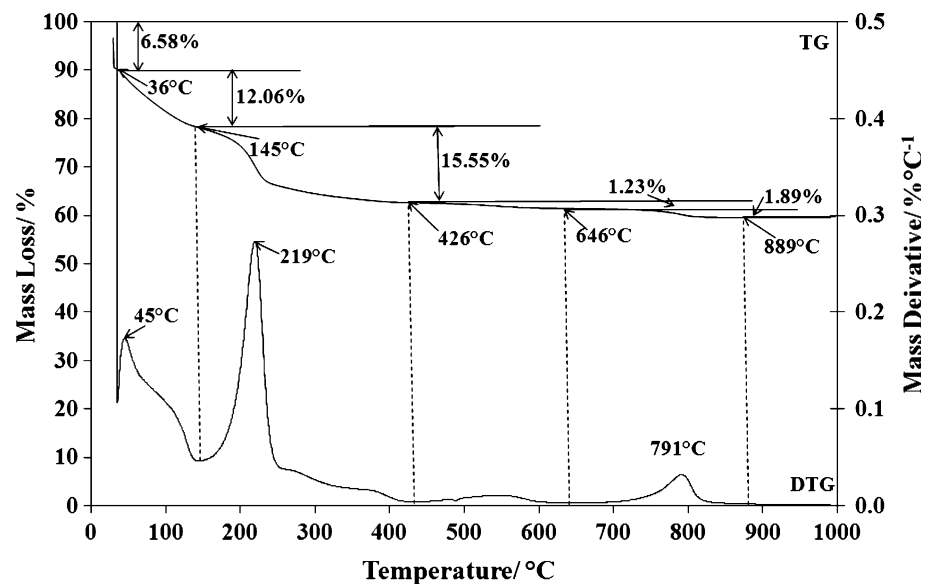


Fig. 4 Thermogravimetric analysis of 40% cobalt doped reevesite (60% Ni)

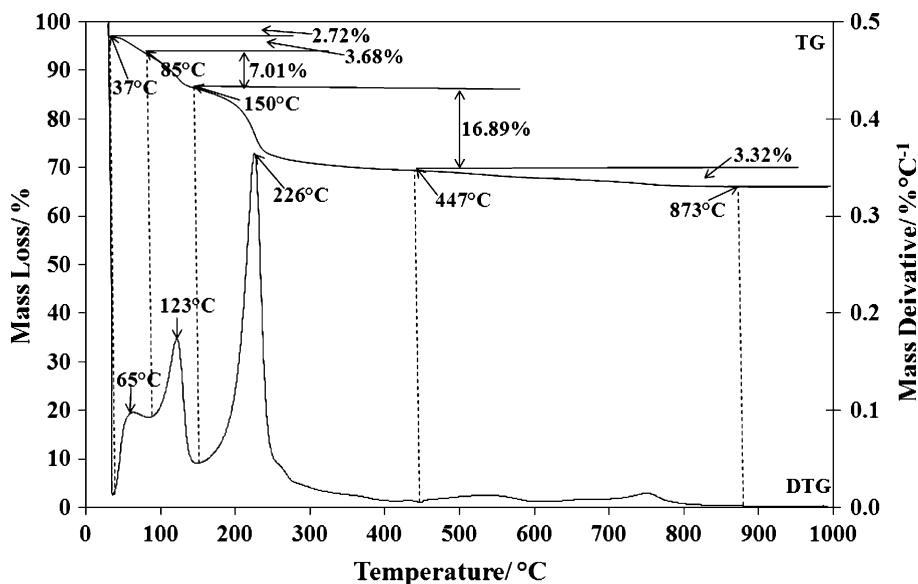
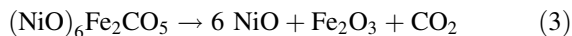
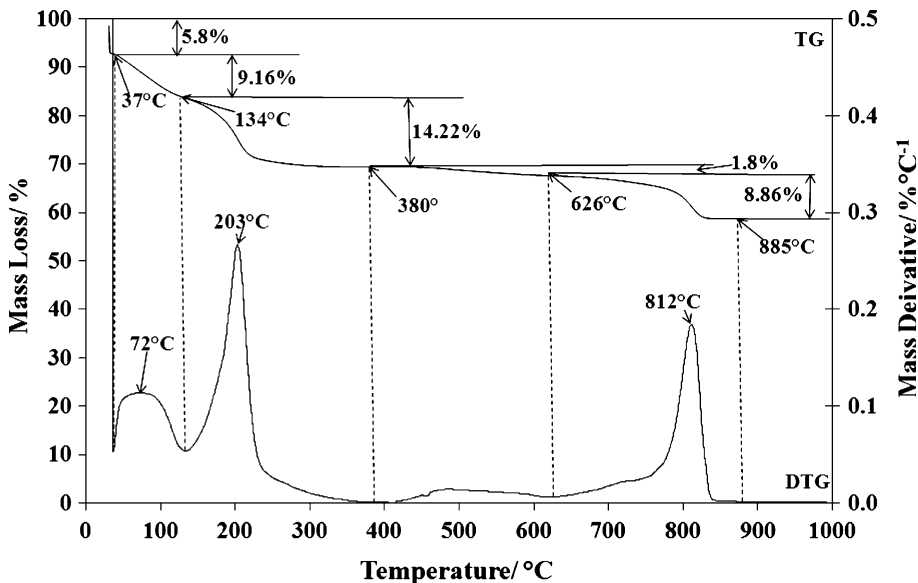


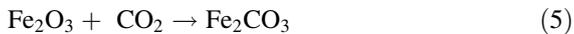
Fig. 5 Thermogravimetric analysis of 60% cobalt doped reevesite (40% Ni)



Further reactions



and



Mass loss step 4 at 807 °C:



And



Implications for the formation of reevesite in meteorite shale balls

The fact that reevesite is found in the inside of shale balls raises the question as to whether the mineral was formed (a) during the space travel of the meteor (b) during impact (c) post-impact. Thermal analysis clearly shows that the thermal stability of reevesite does not surpass around 220 °C. If the mineral was formed pre-impact or during impact, it is unlikely that the mineral would still be present. It is concluded that the reevesite was formed post-impact. The question arises as to how the reevesite was formed. The mineral is present in many parts of Western Australia

Fig. 6 Thermogravimetric analysis of 80% cobalt doped reevesite (20% Ni)

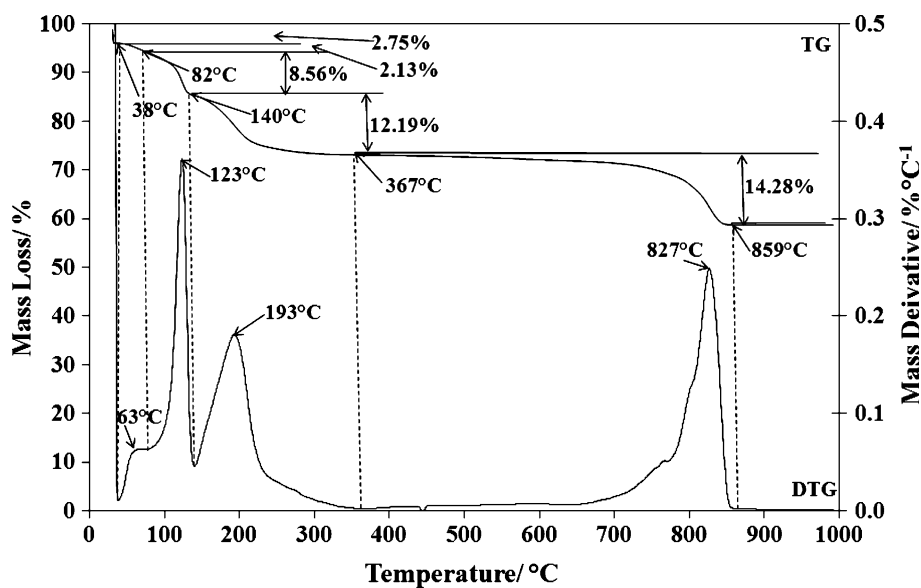
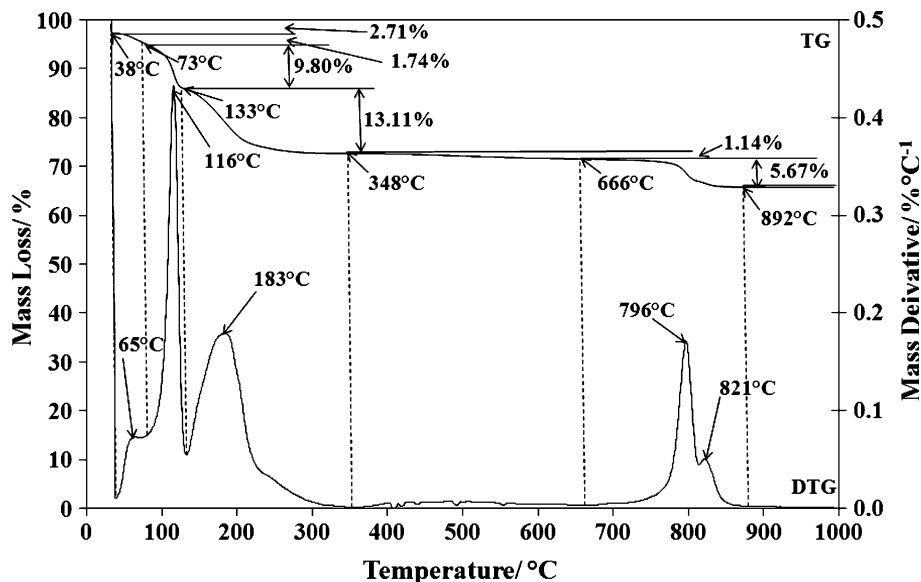


Fig. 7 Thermogravimetric analysis of 100% cobalt doped reevesite (0% Ni)



as there are many nickel containing mineral deposits. If the shale balls contained cracks, then moisture, carbon dioxide could penetrate the interior of the shale ball. The interior of the shale ball will corrode and a range of minerals including the oxides of Fe and Ni could be formed. It is suggested that the mineral reevesite was formed from solution in the interior of the shale balls.

Conclusions

In order to determine the thermal stability of natural reevesite, reevesite and the cobalt substituted reevesites were synthesised. The layered structure of the reevesite

was confirmed by X-ray diffraction. The maximum inter-layer distance occurred when there is maximum substitution of Co for Ni.

Thermogravimetric analysis proves there are at least four decomposition steps attributed to dehydration, dehydroxylation and decarbonation, decomposition of the formed carbonate. The maximum thermal stability occurs for the unsubstituted reevesite and is around 220 °C. A mechanism for the thermal decomposition of reevesite is proposed.

Acknowledgements The financial and infra-structure support of the Queensland University of Technology Inorganic Materials Research Program is gratefully acknowledged. The Australian Research Council (ARC) is thanked for funding the Thermal Analysis Facility.

References

- Allmann R. Crystal structure of pyroaurite. *Acta Crystallogr B*. 1968;24:972–7.
- Ingram L, Taylor HFW. Crystal structures of sjoegrenite and pyroaurite. *Miner Mag J Miner Soc (1876–1968)*. 1967;36:465–79.
- Taylor HFW. Crystal structures of some double hydroxide minerals. *Miner Mag*. 1973;39:377–89.
- Rives V, editor. Layered double hydroxides: present and future, 2001.
- Brown G, Van Oosterwyck-Gastuche MC. Mixed magnesium–aluminum hydroxides. II. Structure and structural chemistry of synthetic hydroxycarbonates and related minerals and compounds. *Clay Miner*. 1967;7:193–201.
- Taylor HFW. Segregation and cation-ordering in sjoegrenite and pyroaurite. *Miner Mag J Miner Soc (1876–1968)*. 1969;37:338–42.
- Taylor RM. Stabilization of color and structure in the pyroaurite-type compounds iron(II) iron(III) aluminum(III) hydroxycarbonates. *Clay Miner*. 1982;17:369–72.
- Kloprogge JT, Wharton D, Hickey L, Frost RL. Infrared and Raman study of interlayer anions CO_2^{-3} , NO^{-3} , SO_2^{-4} and ClO^{-4} in Mg/Al-hydrotalcite. *Am Mineral*. 2002;87:623–9.
- Nickel EH, Wildman JE. Hydrohonesite—a new hydrated nickel-iron hydroxysulfate mineral; its relationship to honessite, carrboydite, and minerals of the pyroaurite group. *Mineral Mag*. 1981;44:333–7.
- Bish DL, Livingstone A. The crystal chemistry and paragenesis of honessite and hydrohonesite: the sulfate analogs of reevesite. *Mineral Mag*. 1981;44:339–43.
- Nickel EH, Clarke RM. Carrboydite, a hydrated sulfate of nickel and aluminum: a new mineral from Western Australia. *Am Mineral*. 1976;61:366–72.
- Chen M, Xie X, El Goresy A. A shock-produced (Mg, Fe)SiO₃ glass in the Suizhou meteorite. *Meteorit Planet Sci*. 2004;39:1797–808.
- Edwards HGM, Farwell DW, Grady MM, Wynn-Williams DD, Wright IP. Comparative Raman microscopy of a Martian meteorite and Antarctic lithic analogues. *Planet Space Sci*. 1999;47:353–62.
- Miyamoto M. Micro Raman spectroscopy of diamonds in the Canyon Diablo iron meteorite: implication for the shock origin. *Antarct Meteor Res*. 1998;11:171–7.
- Miyamoto M, Ohsumi K. Micro Raman spectroscopy of olivines in L6 chondrites: evaluation of the degree of shock. *Geophys Res Lett*. 1995;22:437–40.
- Heymann D. Raman study of olivines in 37 heavily and moderately shocked ordinary chondrites. *Geochim et Cosmochim Acta*. 1990;54:2507–10.
- Van de Moortele B, Reynard B, McMillan PF, Wilson M, Beck P, Gillet P, et al. Shock-induced transformation of olivine to a new metastable (Mg,Fe)²SiO₄ polymorph in Martian meteorites. *Earth Planet Sci Lett*. 2007;261:469–75.
- Wang A, Kuebler KE, Jolliff BL, Haskin LA. Raman spectroscopy of Fe-Ti-Cr-oxides, case study: Martian meteorite EETA79001. *Am Mineral*. 2004;89:665–80.
- White JS Jr, Henderson EP, Mason B. Secondary minerals produced by weathering of the Wolf Creek meteorite. *Am Mineral*. 1967;52:1190–7.
- Faust GT, Fahey JJ, Mason B, Dwornik EJ. Pecoraite, Ni₆Si₄O₁₀(OH)₈, nickel analog of clinochrysotile, formed in the Wolf Creek meteorite. *Science* 1969;165:59–60.
- Frost RL, Reddy BJ, Dickfos MJ. Raman spectroscopy of the nickel silicate mineral pecoraite—an analogue of chrysotile (asbestos). *J Raman Spectrosc*. 2008;39:909–13.
- Kloprogge JT, Hammond M, Frost RL. Low temperature synthesis and characterisation of pecoraite, a nickel containing phyllosilicate. *Neues Jahrbuch fuer Mineralogie, Monatshefte (2000)* 193–206.
- Bouzaid JM, Frost RL, Musumeci AW, Martens WN. Thermal decomposition of the synthetic hydrotalcite woodallite. *J Therm Anal Calorim*. 2006;86:745–9.
- Frost RL, Bouzaid JM, Musumeci AW, Kloprogge JT, Martens WN. Thermal decomposition of the synthetic hydrotalcite iowaite. *J Therm Anal Calorim*. 2006;86:437–41.
- Frost RL, Kristof J, Martens WN, Weier ML, Horvath E. Thermal decomposition of sabugalite. *J Therm Anal Calorim*. 2006;83:675–9.
- Frost RL, Musumeci AW, Kloprogge JT, Weier ML, Adebajo MO, Martens W. Thermal decomposition of hydrotalcite with hexacyanoferrate(II) and hexacyanoferrate(III) anions in the interlayer. *J Therm Anal Calorim*. 2006;86:205–9.
- Frost RL, Wills R-A, Kloprogge JT, Martens W. Thermal decomposition of ammonium jarosite (NH₄)Fe₃(SO₄)₂(OH)₆. *J Therm Anal Calorim*. 2006;84:489–96.
- Frost RL, Wills R-A, Kloprogge JT, Martens WN. Thermal decomposition of hydronium jarosite (H₃O)Fe₃(SO₄)₂(OH)₆. *J Therm Anal Calorim*. 2006;83:213–8.
- Frost RL, Weier ML, Martens W. Thermal decomposition of jarosites of potassium, sodium and lead. *J Therm Anal Calorim*. 2005;82:115–8.
- Lin Y-H, Adebajo MO, Frost RL, Kloprogge JT. Thermogravimetric analysis of hydrotalcites based on the takovite formula Ni_xZn_{6-x}Al₂(OH)₁₆(CO₃) · 4H₂O. *J Therm Anal Calorim*. 2005;81:83–9.
- Kagunya W. Clays for Our Future, Proceedings of the International Clay Conference, 11th, Ottawa, Ont., June 15–21, 1997 (1997) 167–171.